(Received 2 May 2024, Accepted 31 May 2024, Scheduled 16 June 2024)

Common-Mode Voltage Analyses for Space Vector PWM Based on Double Fourier Series

Jian Zheng*, Cunxing Peng, Liangshuai Lin, and Kaihui Zhao

College of Electrical and Information Engineering, Hunan University of Technology, Zhuzhou 412007, China

ABSTRACT: Space vector pulse width modulation (SVPWM) is widely used in three-phase inverters. As the performance requirements of inverters increase, there is a demand to suppress common-mode voltages (CMVs) generated by SVPWM. In order to suppress the CMVs, it is necessary to mathematically analyze the CMVs. By using a mathematical analysis method based on double Fourier series, general expressions of CMV harmonic amplitudes and spectra are obtained for seven-segment SVPWM and five-segment SVPWM. Comparative analyses on the CMV general expressions are performed for the two SVPWMs, and the CMV harmonics characteristics for the two SVPWMs are summarized. Simulations are carried out in an inverter-driven permanent magnet motor system, and simulation results are in good agreement with calculation ones, which verifies the correctness and validity of the mathematical analysis. Based on these analyses, a more in-depth research can be conducted on the CMV suppression.

1. INTRODUCTION

The space vector pulse width modulation (SVPWM) method is the most popular modulation method used for inverters currently [1]. As with other PWM methods, SVPWM also generates common-mode voltages (CMVs) which are jump-stepped voltages [2, 3]. With the application of wide-bandwidth devices and the development of high frequency in inverters, CMVs exacerbate the negative effects such as leakage current, device stress, and electromagnetic interference; therefore, CMV suppression is required in high-performance applications [4–6]. There are two methods for CMV suppression, hardware method and software method. Both hardware and software methods require an in-depth understanding of the CMV characteristics, and the mathematical analyses of CMV harmonics and spectra are the key foundation [7, 8].

Ref. [9] made a spectral analysis of phase voltages and line voltages of SVPWM and carrier-based PWM for three-phase two-level inverters by using double Fourier series. Ref. [10] analyzed harmonic characteristics of carrier-based PWM in three-phase multilevel inverters using double Fourier series. These researches have analyzed the output voltage of three-phase converters with different levels for different carriers, but the CMV spectra have not been analyzed. In [11], CMVs under near-state PWM, discontinuous PWM, and SVPWM methods are analyzed. In [12], CMVs under SVPWM, two discontinuous PWMs, and active zero-state PWM methods are analyzed. These researches performed CMV spectral analysis of three-phase two-level inverters but did not give the CMV specific expressions of the double Fourier series expansion.

In addition, [13] used double Fourier integral method to estimate the harmonics of uncontrolled rectifiers and derived the mathematical expression of harmonic current. Refs. [14, 15] analyzed the output voltage harmonic spectra of five-phase and seven-phase voltage source inverters using double Fourier series analysis. Ref. [16] analyzed the output voltage harmonics of space vector modulation matrix converters using triple Fourier series. Ref. [17] conducted an in-depth analysis of the voltage spectrum of chaotic SPWM in single-phase inverters.

On this basis, this paper investigates the CMVs of seven-section SVPWM and five-section SVPWM for three-phase two-level inverters using the mathematical analytical method of double Fourier series. The general analytical expressions characterizing CMV harmonic amplitudes and spectra are derived. A comparative analysis of the CMV expressions of two SVPWMs is carried out, and the CMV harmonics characteristics of the two SVPWMs are summarized. Further simulations are carried out in an inverter-driven permanent magnet motor system, and simulation results are compared with calculated ones to verify the correctness and validity of the mathematical analyses.

2. CMV WAVE FORMS OF TWO SVPWM METHODS

The CMV u_{cm} of a three-phase two-level inverter is shown in Fig. 1 and is defined as the potential difference between the star junction of the three-phase load and the midpoint z of the dc bus, which is calculated as follows [18]

$$u_{\mathrm{cm}} = \frac{(u_{\mathrm{az}} + u_{\mathrm{bz}} + u_{\mathrm{cz}})}{3} \tag{1}$$

where u_{az}, u_{bz}, and u_{cz} are the voltages of the bridge arms of inverter phases a, b, and c, respectively.

The inverter has eight switching states which correspond to eight fundamental vectors in the α-β plane, denoted as $\mathbf{V}_0$ to $\mathbf{V}_7$, as shown in Fig. 2(a) where $\mathbf{V}_0$ and $\mathbf{V}_7$ are zero vectors,

* Corresponding author: Jian Zheng (zj11660@hut.edu.cn).

doi:10.2528/PIERL24050201

Published by THE ELECTROMAGNETIC ACADEMY

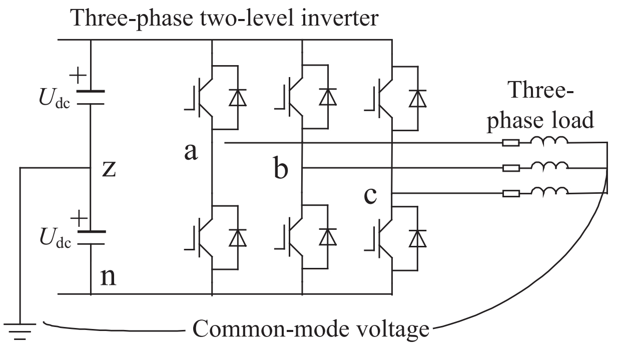

FIGURE 1. Common-mode voltage (CMV) of three-phase two-level inverter.

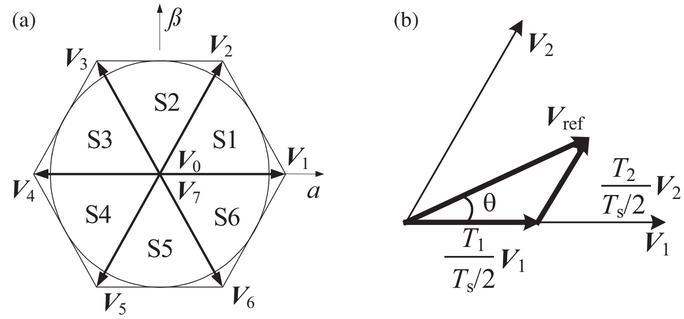

FIGURE 2. Three-phase two-level inverter SVPWM. (a) Basic vectors and sectordivision. (b) Synthesis of reference vector

and $\mathbf{V}_1$ to $\mathbf{V}_6$ are non-zero vectors. The plane is divided into six sectors, denoted as S1 to S6, with non-zero vectors as the boundary.

The reference vector $\mathbf{V}_{\text{ref}}$ is synthesized in sector S1 as shown in Fig. 2(b), and the action times of the effective vectors $\mathbf{V}_1$ and $\mathbf{V}_2$ are denoted by T_1 and T_2 in half of a switching cycle $T_s/2$. The volt-second balance equations are as follows

$$\mathbf{V}_{\text{ref}} = V_{\text{ref}}\angle\theta = \left(\frac{2T_1}{T_{\text{s}}}\right)\mathbf{V}_1 + \left(\frac{2T_2}{T_{\text{s}}}\right)\mathbf{V}_2 \qquad (2)$$

where V_{ref} is the length of $\mathbf{V}_{\text{ref}}$, and θ is the angle between $\mathbf{V}_{\text{ref}}$ and sector start edge. This formula is also suitable for other sectors.

The CMV magnitudes of eight basic vectors are calculated according to (1) and are shown in Table 1. In Table 1, U_{dc} is half of the dc bus voltage.

TABLE 1. CMV magnitudes of eight basic vectors.

$\mathbf{V}_0$	$\mathbf{V}_1$	$\mathbf{V}_2$	$\mathbf{V}_3$	$\mathbf{V}_4$	$\mathbf{V}_5$	$\mathbf{V}_6$	$\mathbf{V}_7$
$-U_{\text{dc}}$	$-U_{\text{dc}}/3$	$U_{\text{dc}}/3$	$-U_{\text{dc}}/3$	$U_{\text{dc}}/3$	$-U_{\text{dc}}/3$	$U_{\text{dc}}/3$	U_{dc}

As can be seen from Table 1, CMVs of the zero vectors are maximum; therefore to reduce the CMVs, the use of zero vectors should be reduced. The seven-segment SVPWM uses $\mathbf{V}_0$ at the beginning and end of switching cycle T_s, and $\mathbf{V}_7$ at the middle segment. The impulse waveforms in sector S1 are shown in Fig. 3(a) where the action times of $\mathbf{V}_0$ and $\mathbf{V}_7$ are denoted as T_0 and T_7. In contrast, the five-segment SVPWM uses only $\mathbf{V}_0$ at the beginning and end of the switching cycle, as shown in Fig. 3(b).

The CMV waveforms of seven-segment SVPWM and five-segment SVPWM in six sectors are shown in Fig. 4. For simplicity, the waveforms of only one switching cycle are plotted in each sector, and the waveforms of other switching cycles are similar.

Comparing Figs. 4(a) and (b), it can be seen that there are differences between the CMV waveforms of two SVPWMs. The first difference is the CMV peak value and valley value of seven-segment SVPWM are U_{dc} and $-U_{\text{dc}}$, respectively, and the peak-valley value is $2U_{\text{dc}}$, while those of five-segment SVPWM are $U_{\text{dc}}/3$ and $-U_{\text{dc}}$, respectively, and the peak-valley value is $4U_{\text{dc}}/3$. The second difference is the number of the CMV jumps of seven-segment SVPWM is 6 in

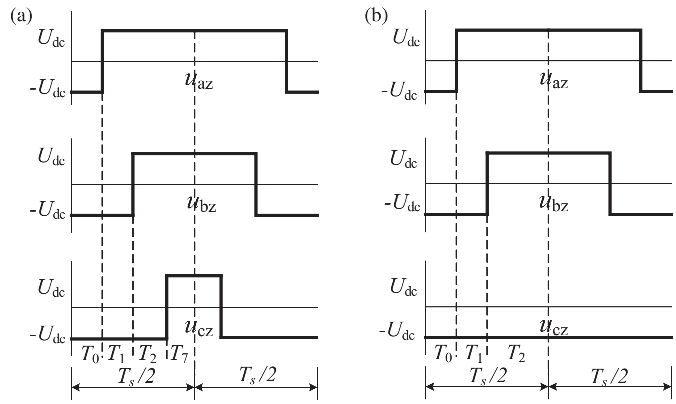

FIGURE 3. Two SVPWM pulse styles. (a) Seven-segment SVPWM. (b) Five-segment SVPWM.

one switching cycle, while that of five-segment SVPWM is 4. The reasons for these differences are the former uses two zero vectors $\mathbf{V}_0$ and $\mathbf{V}_7$, while the latter uses only one zero vector $\mathbf{V}_0$. Since the common-mode voltage jumping can generate high $\mathrm{d}u/\mathrm{d}t$, which is harmful to the system, the fewer the number of common-mode voltage jumps is, the smaller the negative impact is on the system. It can be seen that the five-segment SVPWM is superior to the seven-segment SVPWM from the point of view of suppressing CMV. The mathematical analyses of the CMVs of two SVPWMs by using double Fourier series are as follows.

3. CMV MATHEMATICAL ANALYSES OF TWO SVPWM METHODS

The action times T_1 and T_2 of effective vectors $\mathbf{V}_1$ and $\mathbf{V}_2$ of the two SVPWMs are introduced by (2) as follows

$$\begin{cases} T_1 = \frac{V_{\text{ref}}\sqrt{3}\cos(\theta+\pi/6)}{2U_{\text{dc}}}\cdot\frac{T_{\text{s}}}{2} \\ T_2 = \frac{V_{\text{ref}}\sqrt{3}\cos(\theta-\pi/6)}{2U_{\text{dc}}}\cdot\frac{T_{\text{s}}}{2} \end{cases} \qquad (3)$$

Taking five-segment SVPWM as an example, from Fig. 3(b), the average values of three-phase bridge arm voltages are calculated as follows

$$\begin{cases} \langle u_{\text{az}}\rangle = U_{\text{dc}}\frac{2}{T_{\text{s}}}\left(T_1+T_2-T_0\right) \\ \langle u_{\text{bz}}\rangle = U_{\text{dc}}\frac{2}{T_{\text{s}}}\left(-T_1+T_2-T\right) \\ \langle u_{\text{cz}}\rangle = U_{\text{dc}}\frac{2}{T_{\text{s}}}\left(-T_1-T_2-T_0\right) \end{cases} \qquad (4)$$

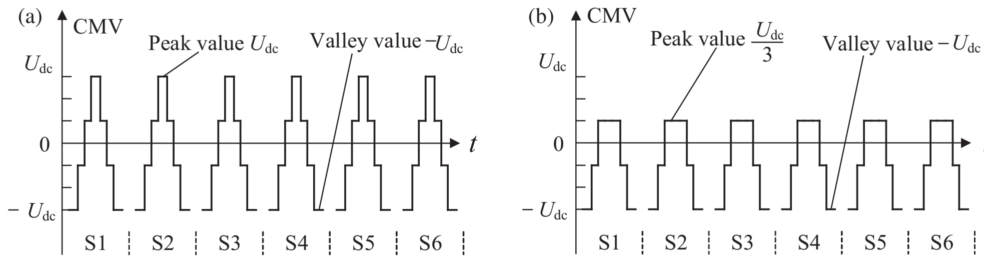

FIGURE 4. CMV waveforms of two SVPWMs. (a) Seven-segment SVPWM. (b) Five-segment SVPWM.

TABLE 2. Double Fourier integration limits of five-segment SVPWM.

i	$y_s(i)$	$y_e(i)$	$x_r(i)$	$x_f(i)$
1	$2\pi/3$	π	0	0
2	0	$2\pi/3$	$-\pi\sqrt{3}M\cos(y-\pi/6)/2$	$\pi\sqrt{3}M\cos(y-\pi/6)/2$
3	$-2\pi/3$	0	$-\pi\sqrt{3}M\cos(y+\pi/6)/2$	$\pi\sqrt{3}M\cos(y+\pi/6)/2$
4	$-\pi$	$-2\pi/3$	0	0

Substituting (3) into (4) yields

$$\begin{cases} \langle u_{\text{az}}\rangle = U_{\text{dc}}\left[\sqrt{3}M\cos\left(\theta_0-\pi/6\right)-1\right] \\ \langle u_{\text{bz}}\rangle = U_{\text{dc}}\left[\sqrt{3}M\cos\left(\theta_0-\pi/2\right)-1\right] \\ \langle u_{\text{cz}}\rangle = -U_{\text{dc}} \end{cases} \tag{5}$$

Examining the voltage u_{an} between the point a of the bridge arm and the point n of the dc bus, according to the principle of double Fourier series, u_{an} is a binary function $u(x,y)$, and independent variables x, y are following two cycle time variables

$$\begin{cases} x\left(t\right) = \omega_c t+\theta_c \\ y\left(t\right) = \omega_0 t+\theta_0 \end{cases} \tag{6}$$

where ω_c and θ_c are the angular frequency and initial phase of the carrier wave, respectively; ω_0 and θ_0 are the angular frequency and initial phase of the fundamental wave, respectively. $u(x,y)$ can be decomposed as follows

$$\begin{aligned} u\left(x,y\right) &= \frac{A_{00}}{2}+\sum_{n=1}^{\infty}\left[A_{0n}\cos\left(ny\right)+B_{0n}\sin\left(ny\right)\right] \\ &\quad +\sum_{m=1}^{\infty}\left[A_{m0}\cos\left(mx\right)+B_{m0}\sin\left(mx\right)\right] \\ &\quad +\sum_{m=1}^{\infty}\sum_{n=\pm1}^{\pm\infty}\left[A_{mn}\cos\left(mx+ny\right)\right. \\ &\quad \left.+B_{mn}\sin\left(mx+ny\right)\right] \end{aligned} \tag{7}$$

The SVPWM output waveforms are spread over six sectors, so the calculating expression of the coefficients in (8) is

$$A_{mn}+jB_{mn} = \frac{1}{2\pi^2}\sum_{i=1}^{6}\int_{y_s(i)}^{y_e(i)}\int_{x_r(i)}^{x_f(i)} 2U_{\text{dc}}e^{j(mx+ny)}\mathrm{d}x\mathrm{d}y \tag{8}$$

The upper and lower limits of integration in (8) are given in Table 2. When $m=n=0$, Equation (8) can be reduced to

$$A_{00}+jB_{00} = \frac{3\sqrt{3}MU_{\text{dc}}}{\pi} \tag{9}$$

where M is the modulation regime, which is defined as the ratio of the reference vector magnitude to half of the dc bus voltage.

When $m=0$ and $n>0$, Equation (8) can be reduced to

$$A_{0n}+jB_{0n} = -\frac{2\sqrt{3}MU_{\text{dc}}}{\pi\left(n^2-1\right)}\left(\cos n\frac{2\pi}{3}+\frac{1}{2}\right) \quad n=3,9,15\ldots \tag{10}$$

where when $n=1$, Equation (10) can be reduced to

$$A_{01}+jB_{01} = MU_{\text{dc}} \tag{11}$$

When $m>0$ and $n\geq0$, Equation (8) can be reduced to

$$A_{mn}+jB_{mn} = \frac{8U_{\text{dc}}}{m\pi^2}\left\{\begin{array}{l} \frac{\pi}{3}\sin n\frac{\pi}{2}\cos n\frac{\pi}{6}J_n\left(m\frac{\sqrt{3}\pi}{2}M\right) \\ +\sum\limits_{\substack{k=1 \\ (k\neq-n)}}^{\infty}\frac{1}{(n+k)}\sin\left[(n+k)\frac{\pi}{3}\right] \\ \sin k\frac{\pi}{2}\cos\left[(2n+k)\frac{\pi}{6}\right]J_k\left(m\frac{\sqrt{3}\pi}{2}M\right) \\ +\sum\limits_{\substack{k=1 \\ (k\neq n)}}^{\infty}\frac{1}{(n-k)}\sin\left[(n-k)\frac{\pi}{3}\right] \\ \sin k\frac{\pi}{2}\cos\left[(2n-k)\frac{\pi}{6}\right]J_k\left(m\frac{\sqrt{3}\pi}{2}M\right) \end{array}\right\} \tag{12}$$

Examining the voltage u_{az} between point a of the bridge arm and point z of the dc bus, its double Fourier expansion is as follows, by subtracting U_{dc} from the dc compensation term of the u_{an} expansion.

$$u_{az} = \frac{\left(3\sqrt{3}M-2\pi\right)U_{\text{dc}}}{2\pi}+\sum_{n=1}^{\infty}A_{0n}\cos\left(n\omega_0 t\right)$$

$$+\sum_{m=1}^{\infty}\sum_{n=-\infty}^{\infty}A_{\text{mn}}\cos\left(m\omega_c t+n\omega_0 t\right) \tag{13}$$

Based on (13), the double Fourier expansions of u_{bz}, u_{cz} can be given by

$$\begin{aligned}u_{bz}=&\frac{\left(3\sqrt{3}M-2\pi\right)U_{\text{dc}}}{2\pi}+\sum_{n=1}^{\infty}A_{0\text{n}}\cos\left[n\left(\omega_0 t+\frac{2\pi}{3}\right)\right]\\&+\sum_{m=1}^{\infty}\sum_{n=-\infty}^{\infty}A_{\text{mn}}\cos\left[m\omega_c t+n\left(\omega_0 t+\frac{2\pi}{3}\right)\right]\\u_{cz}=&\frac{\left(3\sqrt{3}M-2\pi\right)U_{\text{dc}}}{2\pi}+\sum_{n=1}^{\infty}A_{0\text{n}}\cos\left[n\left(\omega_0 t-\frac{2\pi}{3}\right)\right]\\&+\sum_{m=1}^{\infty}\sum_{n=-\infty}^{\infty}A_{\text{mn}}\cos\left[m\omega_c t+n\left(\omega_0 t-\frac{2\pi}{3}\right)\right]\end{aligned} \tag{14}$$

Combining (13) and (14), the CMV double Fourier expansion of five-segment SVPWM is obtained

$$\begin{aligned}u_{\text{cm}}=&\left(u_{\text{az}}+u_{\text{bz}}+u_{\text{cz}}\right)/3\\=&\frac{\left(3\sqrt{3}M-2\pi\right)U_{\text{dc}}}{2\pi}-\frac{2\sqrt{3}MU_{\text{dc}}}{\pi}\\&\sum_{n=3,9,15\ldots}^{\infty}\frac{1}{(n^2-1)}\left(\cos n\frac{2\pi}{3}+\frac{1}{2}\right)G(t)\\&+\frac{8U_{\text{dc}}}{\pi^2}\sum_{m=1}^{\infty}\sum_{n=-\infty}^{\infty}\frac{1}{m}\\&\left\{\begin{array}{l}\frac{\pi}{3}\sin n\frac{\pi}{2}\cos n\frac{\pi}{6}J_n\left(m\frac{\sqrt{3}\pi}{2}M\right)\\+\sum\limits_{\substack{k=1\\(k\neq -n)}}^{\infty}\frac{1}{(n+k)}\sin\left[(n+k)\frac{\pi}{3}\right]\\\sin k\frac{\pi}{2}\cos\left[(2n+k)\frac{\pi}{6}\right]J_k\left(m\frac{\sqrt{3}\pi}{2}M\right)\\+\sum\limits_{\substack{k=1\\(k\neq n)}}^{\infty}\frac{1}{(n-k)}\sin\left[(n-k)\frac{\pi}{3}\right]\\\sin k\frac{\pi}{2}\cos\left[(2n-k)\frac{\pi}{6}\right]J_k\left(m\frac{\sqrt{3}\pi}{2}M\right)\end{array}\right\}H(t)\end{aligned} \tag{15}$$

where

$$\begin{aligned}G(t)=&\frac{1}{3}\left\{\cos n\omega_0 t+\cos\left[n\left(\omega_0 t+\frac{2\pi}{3}\right)\right]\right.\\&\left.+\cos\left[n\left(\omega_0 t-\frac{2\pi}{3}\right)\right]\right\}\\H(t)=&\frac{1}{3}\left\{\cos\left(m\omega_c t+n\omega_0 t\right)+\cos\left[m\omega_c t+n\left(\omega_0 t+\frac{2\pi}{3}\right)\right]\right.\\&\left.+\cos\left[m\omega_c t+n\left(\omega_0 t-\frac{2\pi}{3}\right)\right]\right\}\end{aligned}$$

Similarly, the CMV double Fourier expansion of seven-segment SVPWM is obtained

$$\begin{aligned}u_{\text{cm}}=&\frac{3\sqrt{3}MU_{\text{dc}}}{\pi}\sum_{n=3,9,15,\ldots}^{\infty}\frac{1}{n^2-1}\left(\cos n\frac{2\pi}{3}+1\right)G(t)\\&+\frac{8U_{\text{dc}}}{\pi^2}\sum_{m=1}^{\infty}\sum_{n=-\infty}^{\infty}\frac{1}{m}\\&\left\{\begin{array}{l}\frac{\pi}{6}\sin\left[(m+n)\frac{\pi}{2}\right]\left[J_n\left(m\frac{3\pi}{4}M\right)\right.\\\left.+2\cos n\frac{\pi}{6}J_n\left(m\frac{\sqrt{3}\pi}{4}M\right)\right]\\+\frac{1}{n}\sin m\frac{\pi}{2}\cos n\frac{\pi}{2}\sin n\frac{\pi}{6}\\\left.\left[J_0\left(m\frac{3\pi}{4}M\right)-J_0\left(m\frac{\sqrt{3}\pi}{4}M\right)\right]\right|_{n\neq 0}\\+\sum\limits_{\substack{k=1\\k\neq -n}}^{\infty}\left\{\begin{array}{l}\frac{1}{(n+k)}\sin\left[(m+k)\frac{\pi}{2}\right]\\\cos\left[(n+k)\frac{\pi}{2}\right]\sin\left[(n+k)\frac{\pi}{6}\right]\\\times\left\{J_k\left(m\frac{3\pi}{4}M\right)+2\cos\left[(2n+3k)\frac{\pi}{6}\right]\right.\\\left.J_k\left(m\frac{\sqrt{3}\pi}{4}M\right)\right\}\end{array}\right\}\\+\sum\limits_{\substack{k=1\\k\neq n}}^{\infty}\left\{\begin{array}{l}\frac{1}{(n-k)}\sin\left[(m+k)\frac{\pi}{2}\right]\cos\left[(n-k)\frac{\pi}{2}\right]\\\sin\left[(n-k)\frac{\pi}{6}\right]\\\times\left\{J_k\left(m\frac{3\pi}{4}M\right)+2\cos\left[(2n-3k)\frac{\pi}{6}\right]\right.\\\left.J_k\left(m\frac{\sqrt{3}\pi}{4}M\right)\right\}\end{array}\right\}\end{array}\right\}H(t)\end{aligned} \tag{16}$$

The comparison of (15) with (16) shows that there is a dc component in the five-segment SVPWM, while there is no dc component in the seven-segment SVPWM. The low harmonic frequency of the five-segment SVPWM is integer multiples of 3 of the fundamental frequency, while that of the seven-segment SVPWM is odd integer multiples of 3 of the fundamental frequency. Further comparison shows that the five-segment SVPWM has more CMV harmonic components than the seven-segment SVPWM, but the harmonic amplitudes are significantly reduced. This is because the five-segment SVPWM uses only one type of zero vectors, while the seven-segment SVPWM uses two types of zero vectors.

In addition, a general feature of both expressions is that the CMV sideband harmonics only exist at $mf_c \pm nf_0$, with n taking values of integer multiples of 3. As n becomes larger, the sideband harmonic amplitudes decrease, and the magnitudes of these amplitudes are related to the modulation regime M, the number of harmonics, etc.

These features mentioned above can provide a theoretical basis for the design of common-mode filters and CMV suppression strategies.

4. SIMULATION VERIFICATION

To verify the correctness and validity of the above-mentioned analyses, simulations of two SVPWMs are done on an experimental platform of an inverter-driven permanent magnet synchronous motor system, and relevant results are compared. Inverter dc bus voltage is 311 V; switching frequency is 5 kHz; permanent magnet motor rated voltage is 130 V/50 Hz; the number of pole pairs is 4; stator resistance is 0.958 Ω; stator straight-axis inductance is 5.25 mH; cross-axis inductance is 12 mH; rotor magnetic chain is 0.1827 W; rotational inertia is 0.003 kg · m^2; damping coefficient is 0.008 N · m · s. The system uses the closed-loop control, which is the vector control with $i_{\text{d}} = 0$ and a speed command value of 750 r/min. Based on the speed command value and dc bus voltage, it can be seen that the modulation regime is 0.48.

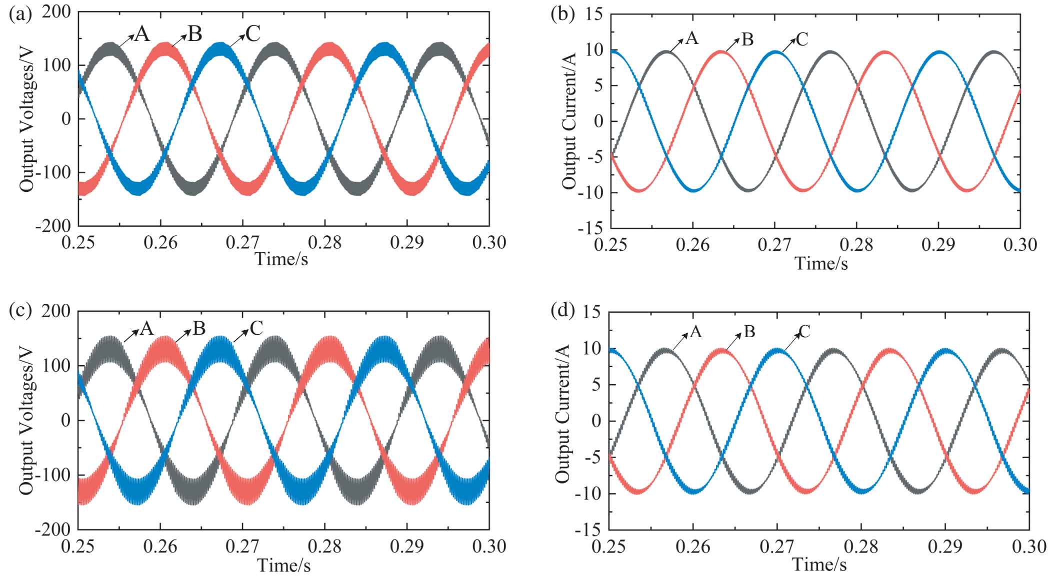

FIGURE 5. Voltage and current simulation waveforms of two SVPWMs. (a) Seven-segment SVPWM line voltage (after low-pass filtering). (b) Seven-segment SVPWM line current. (c) Five-segment SVPWM line voltage (after low-pass filtering). (d) Five-segment SVPWM line current.

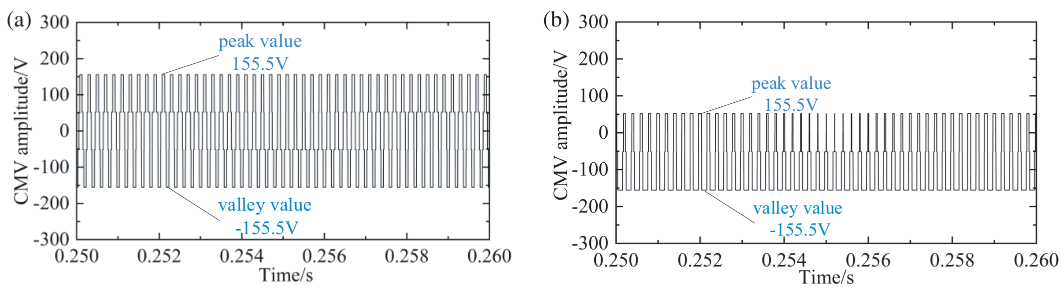

FIGURE 6. CMV simulation waveforms of two SVPWMs. (a) Seven-segment SVPWM. (b) Five-segment SVPWM.

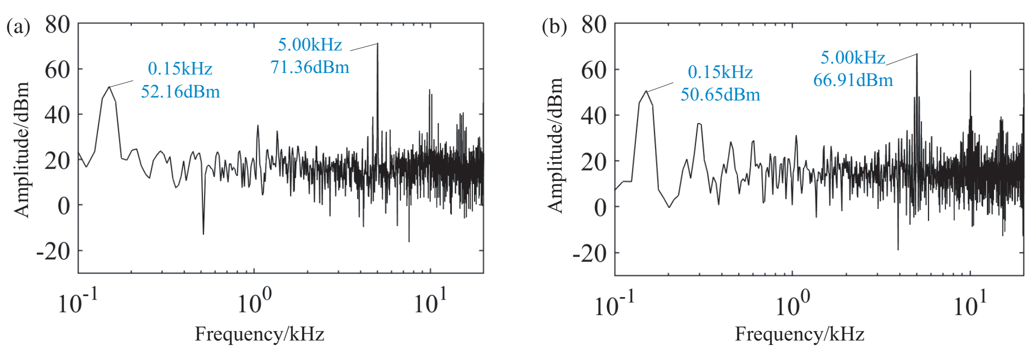

FIGURE 7. CMV spectral analysis results of two SVPWM. (a) Seven-segment SVPWM. (b) Five-segment SVPWM.

Simulation waveforms of line voltages (after low-pass filtering) and line currents of two SVPWMs in steady state are shown in Fig. 5. As can be seen from the figures, the sinusoidal degree of the waveforms is good, and the ripple of five-section SVPWM is more than that of seven-section SVPWM, which is in line with both characteristics.

The CMV simulation waveforms of the two SVPWMs in steady state are shown in Fig. 6. From the figure, it can be seen that the CMV peak-valley value of the seven-segment SVPWM is 311 V, while that of the five-segment SVPWM is 207.33 V, that is a reduction of 33.33%, which is consistent with theoretical analyses.

The CMV spectral analysis results of both SVPWMs in steady state are shown in Fig. 7, which is performed for the whole waveforms of the simulation process. From this figure, it can be seen that at switching frequency 5 kHz, the CMV of seven-segment SVPWM shows 71.36 dBm while the CMV of five-segment SVPWM shows 66.91 dBm, which is a decrease of 4.45 dBm. Meanwhile, at 0.15 kHz, the CMV of seven-segment SVPWM shows 52.16 dBm while the CMV of five-segment SVPWM shows 50.65 dBm, which is a decrease of 1.51 dBm.

TABLE 3. CMV calculated values and simulation values of seven-segment SVPWM.

Frequency/Hz	150	5000	9850	10150	14700	15000	19850	20150
Calculated value/V	15.71	168.54	13.77	13.78	3.27	2.10	9.23	8.99
Simulation value/V	15.59	168.45	13.63	13.78	3.62	2.21	8.89	9.10
Relative error rates %	0.76	0.05	1.03	0	4.14	4.9	3.8	1.2

TABLE 4. CMV calculated values and simulation values of five-segment SVPWM.

Frequency/Hz	0	150	5000	9850	10150	14700	15000	19850	20150
Calculated value/V	92.49	15.71	99.91	4.58	4.59	3.12	2.21	7.09	7.07
Simulation value/V	92.65	15.53	100.14	4.36	4.69	3.41	2.53	7.17	7.13
Relative error rates %	0.17	1.15	0.23	3.44	2.1	2.64	4.35	1.12	0.84

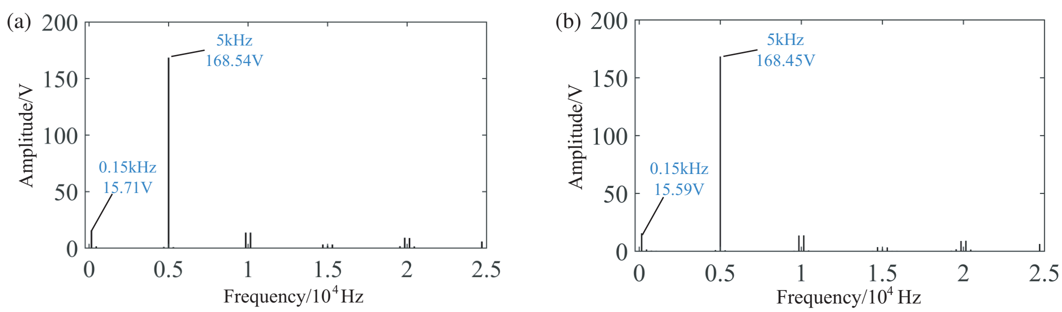

FIGURE 8. CMV calculated spectra and simulation spectra (seven-segment SVPWM). (a) CMV calculated spectrum. (b) CMV simulation spectrum.

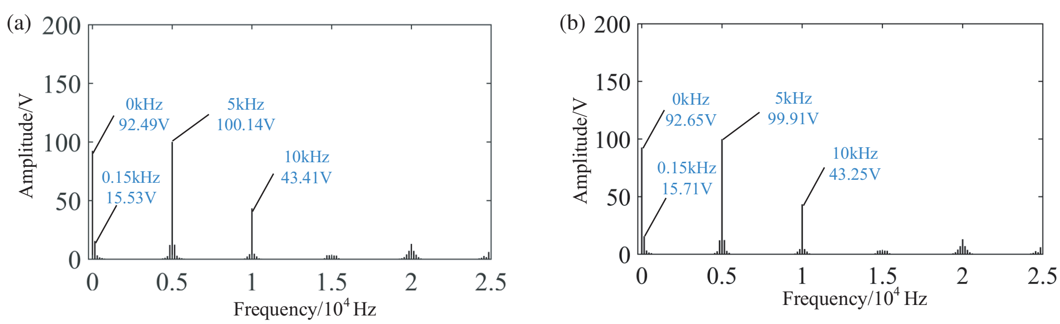

FIGURE 9. CMV calculated spectra and simulation spectra (five-segment SVPWM). (a) CMV calculated spectrum. (b) CMVsimulation spectrum.

By using (16), the CMV calculated results of seven-segment SVPWM can be derived, and a comparison between calculated and simulated values is shown in Table 3, which shows that there is very little error between the two. The CMV calculated and simulated spectra in one fundamental period are shown in Fig. 8, and there is a high degree of agreement between the two. From this, it can be seen that the CMV double Fourier series analysis results mentioned above are correct and effective.

Similarly, by using (15), the CMV calculated results of five-segment SVPWM can be derived, and a comparison between calculated and simulated values is shown in Table 4, and the errors between the two are also very small. Fig. 9 shows the CMV calculated and simulated spectra, which are also in good agreement with each other. It further shows that the above analysis results of the CMV double Fourier series are correct and valid.

5. CONCLUSION

This paper analyzes the CMV waveform characteristics of the seven-segment SVPWM and the five-segment SVPWM for the three-phase two-level inverters. By using double Fourier series, the CMV general analytical expressions of two SVPWMs are derived. By comparing and analyzing the analytical expressions, the characteristics of CMV harmonic amplitudes and frequency spectra of two SVPWMs are obtained. The simulation results have verified the correctness and effectiveness of the theoretical derivation results. These analyses are of great significance for designing common-mode filters and CMV suppression strategies and provide an important reference for CMV analyses of other PWM methods. The research work of this paper mainly focuses on the steady-state CMV waveforms, and the subsequent in-depth analyses of transient CMV waveforms are planned.

REFERENCES

[1] Mirafzal, B., *Power Electronics in Energy Conversion Systems*, McGraw-Hill Education, 2022.

[2] Zheng, J., C. Peng, K. Zhao, and M. Lyu, "A low common-mode SVPWM for two-level three-phase voltage source inverters," *Energies*, Vol. 16, No. 21, 7294, 2023.

[3] Feng, Q., C. Liao, and X.-Z. Xiong, "A novel measurement system for the common-mode-and differential-mode-conducted electromagnetic interference," *Progress In Electromagnetics Research Letters*, Vol. 48, 75–81, 2014.

[4] Hu, Y., S. Cheng, B. Chen, J. Hu, W. Huang, S. Li, and Y. Lv, "A novel leakage-current monitoring method for inverter-fed AC motors," *IEEE Transactions on Industrial Electronics*, 2024, doi: 10.1109/TIE.2024.3360631.

[5] Phukan, R., X. Zhao, P. Asfaux, D. Dong, and R. Burgos, "Investigation of staggered PWM scheme for AC common mode current minimization in SiC-based three-phase inverters," *IEEE Transactions on Transportation Electrification*, Vol. 8, No. 4, 4378–4390, 2022.

[6] Qamar, H., H. Qamar, and R. Ayyanar, "Performance analysis and experimental validation of 240°-clamped space vector PWM to minimize common mode voltage and leakage current in EV/HEV traction drives," *IEEE Transactions on Transportation Electrification*, Vol. 8, No. 1, 196–208, 2022.

[7] Quan, Z. and Y. W. Li, "Impact of PWM schemes on the common-mode voltage of interleaved three-phase two-level voltage source converters," *IEEE Transactions on Industrial Electronics*, Vol. 66, No. 2, 852–864, 2019.

[8] Alcaide, A. M., H. Yan, X. Wang, J. I. Leon, R. Portillo, G. Buticchi, S. Vazquez, V. G. Monopoli, M. Liserre, and L. G. Franquelo, "Common-mode voltage mitigation technique in motor drive applications by applying a sampling-time adaptive multi-carrier PWM method," *IEEE Access*, Vol. 9, 56 115–56 126, 2021.

[9] Holmes, D. G. and T. A. Lipo, *Pulse Width Modulation for Power Converters: Principles and Practice*, John Wiley & Sons, 2003.

[10] Gao, Z., Y. Li, Q. Ge, K. Wang, M. Zhao, and J. Zhu, "Research on the synchronized carrier-based PWM strategy under low switching frequency for three-level neutral point clamped inverter," in *IECON 2020 The 46th Annual Conference of the IEEE Industrial Electronics Society*, 4121–4126, Singapore, Oct. 2020.

[11] Zhang, Y., C. Li, M. Schutten, C. F. D. Leon, and S. Prabhakaran, "Common-mode EMI comparison of NSPWM, DPWM1, and SVPWM modulation approaches," in *2019 IEEE Energy Conversion Congress and Exposition (ECCE)*, 6430–6437, Baltimore, MD, USA, Sep. 2019.

[12] Huang, Y., J. Walden, A. Foote, H. Bai, D. Lu, F. Jin, and B. Cheng, "Analytical characterization of CM and DM performance of three-phase voltage-source inverters under various PWM patterns," *IEEE Transactions on Power Electronics*, Vol. 36, No. 4, 4091–4104, 2020.

[13] Abdelqader, R. O. and D. Robinson, "Double fourier integral method for PWM rectifiers to estimate harmonics of uncontrolled rectifiers," in *2020 19th International Conference on Harmonics and Quality of Power (ICHQP)*, 1–6, Dubai, United Arab Emirates, Jul. 2020.

[14] Hamedani, P., C. Garcia, and J. Rodriguez, "Analytical calculation of harmonics and harmonic losses in five-phase carrier-based PWM voltage source inverters," *IEEE Access*, Vol. 10, 37 330–37 344, 2022.

[15] Hamedani, P., "Harmonic evaluation of seven-phase VSI with PWM switching teqnique," in *2020 11th Power Electronics, Drive Systems, and Technologies Conference (PEDSTC)*, 1–6, Tehran, Iran, Feb. 2020.

[16] Shi, T., L. Wu, Y. Yan, and C. Xia, "Harmonic spectrum of output voltage for space vector-modulated matrix converter based on triple fourier series," *IEEE Transactions on Power Electronics*, Vol. 33, No. 12, 10 646–10 653, 2018.

[17] Li, H., Y. Liu, J. Lü, T. Zheng, and X. Yu, "Suppressing EMI in power converters via chaotic SPWM control based on spectrum analysis approach," *IEEE Transactions on Industrial Electronics*, Vol. 61, No. 11, 6128–6137, 2014.

[18] Jayaraman, K. and M. Kumar, "Design of passive common-mode attenuation methods for inverter-fed induction motor drive with reduced common-mode voltage PWM technique," *IEEE Transactions on Power Electronics*, Vol. 35, No. 3, 2861–2870, 2019.